Available online at www.sciencedirect.com
SCIENCE DIRECT®
PERGAMON
International Journal of Heat and Mass Transfer 47 (2004) 21–30
International Journal of HEAT and MASS TRANSFER
www.elsevier.com/locate/ijhmt

A Fourier transform based data reduction method for the evaluation of the local convective heat transfer coefficient

G.E. Cossali *

Facoltà di Ingegneria, Università degli Studi di Bergamo, Via Marconi 6, 24044 Dalmine (BG), Italy

Received 9 September 2002; received in revised form 14 July 2003

Abstract

A new data reduction technique for measuring the convective heat transfer coefficient is reported. The technique is based on the evaluation of the Fourier transform of simultaneously measured freestream temperature and surface wall temperature or heating power. Any wave shape can be used to heat-up the stream or the wall and the method yields information redundancy on the local heat transfer coefficient. Effects of various uncertainties on the accuracy of the heat transfer coefficient evaluation are considered and quantitatively analysed. A numerical simulation of the effects of noise on the measured temperature signal is also reported and discussed.

1. Introduction

Local convective heat transfer coefficient can be measured by a variety of different methods. Transient methods are widely used since many years, they are all based on the use of the transient temperature of the surface of a model to deduce the local heat flux and heat transfer coefficient. The oldest and more consolidated transient methods use a step change in the temperature difference between the model and the surrounding fluid (see [1,2] for a description of the principles and data reduction techniques for those methods). One dimensional heat conduction is usually assumed and it is considered to be sufficiently accurate specially when the surface has low thermal diffusivity (like for plexiglass or similar materials), in fact, in this case the surface temperature response is limited to a thin layer near the surface and lateral conduction is negligible. The main difficulty in such methods was to accomplish the fluid temperature change relative to surface temperature and many techniques were developed to overcome it, like using switching valves to rise the temperature of the fluid [1–5], preheating the model and inserting it suddenly into place across a channel [6] or initiating the flow using a diverting door [7], removing a shield blocking a heated flat surface from an impinging jet [8].

Von Wolfersdorf et al. [9] introduced a new technique that did not require direct measurements of heat flux and wall temperature, the heat transfer coefficient was deduced from two time measurements and suggested the applicability of more than one heat step to obtain redundancy information, then firstly proposing a sort of periodical technique.

A new type of transient methods was introduced by Baughn et al. [10] where the freestream temperature was periodical heated while the local surface temperature of a model was measured. The local heat transfer coefficient could be determined from the frequency of the periodic change in the freestream temperature, the ratio of the surface temperature changes to the freestream temperature change and model thermal properties. This method avoided the main difficulty of the transient step methods above described. More recently [11] a periodic technique based on the measurement of the phase lag between model surface temperature and surface heating power was introduced. In this case absolute temperature measurements are not required and only phase measurements are necessary, which are usually affected by lower experimental errors.

The present paper introduces a new possibility of measuring heat transfer coefficient by periodic varying

* Tel.: +39-0352052309; fax: +39-03556-2779.
E-mail address: cossali@unibg.it (G.E. Cossali).

0017-9310/$ - see front matter © 2003 Elsevier Ltd. All rights reserved.
doi:10.1016/S0017-9310(03)00388-0

Nomenclature

a, A, b, B	constants	η	fluctuating component of the heat transfer coefficient
c_p	specific heat		
h	convective heat transfer coefficient	θ	temperature fluctuation
Im	imaginary part of a complex value	ξ	non-dimensional position
k	thermal conductivity	ρ	density
L	slab thickness	σ	noise intensity
q	heat flux	τ	non-dimensional time
Re	real part of a complex value	ϕ	phase lag
T	temperature	φ	heat flux fluctuation
t	time	$\dot{\Phi}$	heating power fluctuation
x	position	ω'	frequency
w	wall surface	ω	non-dimensional frequency
Greek symbols		*Indexes*	
α	thermal diffusivity	a	time average
Δ	absolute uncertainty	g	freestream
ε	relative uncertainty	1	values at $x = L$

either the gas temperature or the surface heating power with no imposition about the wave shape and obtaining redundancy information about heat transfer coefficient on a single experiment.

2. Theoretical background

Consider the one-dimensional time dependent conduction in a homogeneous slab of finite thickness L, the heat equation is:

$$\frac{\partial T}{\partial t} = \alpha \frac{\partial^2 T}{\partial x^2} \tag{1}$$

where $\alpha = k/\rho c_p$ is the thermal diffusivity. With the usual positions: $\xi = x/L$, $\tau = t\alpha/L^2$, Eq. (1) becomes

$$\frac{\partial T}{\partial \tau} = \frac{\partial^2 T}{\partial \xi^2} \tag{2}$$

Let us first consider the case when the freestream temperature varies with time, described by the following boundary conditions

$$\begin{aligned} &\xi = 0: \quad q(0,\tau) = h[T_g(\tau) - T(0,\tau)] \\ &\xi = 1: \quad q(1,\tau) = 0 \end{aligned} \tag{3}$$

where $T_g(t)$ is the temperature of the gas stream in contact with the slab surface at $x = 0$, h is the convective heat transfer coefficient and $q(\xi,\tau) = -k\frac{\partial T(\xi,\tau)}{\partial x} = -\frac{k}{L}\frac{\partial T(\xi,\tau)}{\partial \xi}$ is the heat flux. The second of (3) represents the adiabatic condition at $x = L$. Let now decompose the gas and wall temperature in steady and fluctuating parts as:

$$\begin{aligned} T_g(\tau) &= T_{g,a} + \theta_g(\tau) \\ T(\xi,\tau) &= T_a(\xi) + \theta(\xi,\tau) \end{aligned} \tag{4}$$

where $T_{g,a} = \lim_{\Upsilon\to\infty} \frac{1}{\Upsilon}\int_0^{\Upsilon} T_g(\tau)\,d\tau$; $T_a(\xi) = \lim_{\Upsilon\to\infty} \frac{1}{\Upsilon} \times \int_0^{\Upsilon} T(\xi,\tau)\,d\tau$ and the heat flux as:

$$q(\xi,\tau) = q_a(\xi) + \varphi(\xi,\tau) \tag{5}$$

where $q_a(\xi) = \lim_{\Upsilon\to\infty} \frac{1}{\Upsilon}\int_0^{\Upsilon} q(\xi,\tau)\,d\tau$. Consider now the Fourier transforms of the gas and wall fluctuating temperature defined as

$$\begin{aligned} \theta(\xi,\tau) &= \int_{-\infty}^{+\infty} e^{i\omega\tau} S(\omega,\xi)\,d\omega \\ \theta_g(\tau) &= \int_{-\infty}^{+\infty} e^{i\omega\tau} G(\omega)\,d\omega \end{aligned} \tag{6}$$

and for the heat flux

$$\varphi(\xi,\tau) = \int_{-\infty}^{+\infty} e^{i\omega\tau} F(\omega,\xi)\,d\omega$$

where ω is a non-dimensional number related to the dimensional frequency ω' through the relation: $\omega = \omega' L^2/\alpha$. Solving (2) by using the first of Eq. (6)

$$i\omega S(\omega,\xi) = \frac{\partial^2 S(\omega,\xi)}{\partial \xi^2} \tag{7}$$

from which

$$S(\omega,\xi) = S_-(\omega)E_-(\omega,\xi) + S_+(\omega)E_+(\omega,\xi) \tag{8}$$

where $E_\pm(\omega,\xi) = e^{\pm(1+i)\sqrt{\omega/2}}$. The heat flux inside the slab is then

$$F(\omega,\xi)=\frac{k}{L}(1+\mathrm{i})\sqrt{\frac{\omega}{2}}[S_-(\omega)E_-(\omega,\xi)-S_+(\omega)E_+(\omega,\xi)] \tag{9}$$

Applying the boundary conditions (3) one obtains for the steady components:

$$\begin{aligned} &T_\mathrm{a}(\xi)=T_\mathrm{g,a}\\ &q_\mathrm{a}(\xi)=0 \end{aligned} \tag{10}$$

and for the fluctuating components

$$S_+(\omega)=S_-(\omega)\frac{E_-(\omega,1)}{E_+(\omega,1)} \tag{11}$$

$$\begin{aligned} &\frac{k}{L}(1+\mathrm{i})\sqrt{\frac{\omega}{2}}[S_-(\omega)-S_+(\omega)]\\ &\quad=h[G(\omega)-S_-(\omega)-S_+(\omega)] \end{aligned} \tag{12}$$

substituting (11) in (12) and putting $Bi=hL/k$

$$\begin{aligned} &(1+\mathrm{i})\sqrt{\frac{\omega}{2}}S_-(\omega)\left[1-\frac{E_-(\omega,1)}{E_+(\omega,1)}\right]\\ &\quad=Bi\left\{G(\omega)-S_-(\omega)\left[1+\frac{E_-(\omega,1)}{E_+(\omega,1)}\right]\right\} \end{aligned}$$

Now, from Eqs. (8) and (11)

$$S(\omega,0)=S_-(\omega)\left[1+\frac{E_-(\omega,1)}{E_+(\omega,1)}\right] \tag{13}$$

defining the function $Q(\omega)$ by

$$Q(\omega)=\frac{E_+(\omega,1)-E_-(\omega,1)}{E_+(\omega,1)+E_-(\omega,1)} \tag{14}$$

one obtains

$$G(\omega)=S(\omega,0)\left\{\frac{(1+\mathrm{i})}{Bi}\sqrt{\frac{\omega}{2}}Q(\omega)+1\right\} \tag{15}$$

Observing that

$$\begin{aligned} (1+\mathrm{i})Q(\omega)&=[Q_\mathrm{r}(\omega)-Q_\mathrm{i}(\omega)]+\mathrm{i}[Q_\mathrm{r}(\omega)+Q_\mathrm{i}(\omega)]\\ &=K^-(\omega)+\mathrm{i}K^+(\omega) \end{aligned} \tag{16}$$

with $Q_\mathrm{r}(\omega)=\mathrm{Re}(Q(\omega))$ and $Q_\mathrm{i}(\omega)=\mathrm{Im}(Q(\omega))$, $K^\pm(\omega)=[Q_\mathrm{r}(\omega)\pm Q_\mathrm{i}(\omega)]$; from Eq. (15) it is possible to obtain

$$\mathrm{Re}[S(\omega,0)G^*(\omega)]=\frac{|S(\omega,0)|^2}{Bi}\left\{Bi+\sqrt{\frac{\omega}{2}}K^-(\omega)\right\}$$

$$\mathrm{Im}[S(\omega,0)G^*(\omega)]=-\frac{|S(\omega,0)|^2}{Bi}\left\{\sqrt{\frac{\omega}{2}}K^+(\omega)\right\}$$

with $G^*(\omega)$ complex conjugate of $G(\omega)$. Finally

$$W(\omega)=\frac{\mathrm{Re}[S(\omega,0)G^*(\omega)]}{\mathrm{Im}[S(\omega,0)G^*(\omega)]}=-\left\{\frac{Bi}{\sqrt{\frac{\omega}{2}}K^+(\omega)}+\frac{K^-(\omega)}{K^+(\omega)}\right\}$$

or

$$Bi=-\sqrt{\frac{\omega}{2}}\{K^-(\omega)+K^+(\omega)W(\omega)\} \tag{17}$$

Eq. (17) gives a relation that allows to evaluate Bi (and then the local convective heat transfer coefficient) from the Fourier transform of the wall surface temperature and the gas temperature. It should be noticed that, defining the freestream–wall temperature crosscorrelation:

$$\mathscr{C}(\tau)=\int_{-\infty}^{+\infty}\theta(0,t+\tau)\theta_\mathrm{g}(t)\,\mathrm{d}t$$

the convolution theorem for Fourier transform (see, for example [12,13]) gives

$$\mathscr{C}(\tau)=\int_{-\infty}^{+\infty}\mathrm{e}^{\mathrm{i}\omega\tau}S(\omega,0)G^*(\omega)\,\mathrm{d}\omega$$

thus $W(\omega)$ can also be evaluated from the real and imaginary components of the Fourier transform of $\mathscr{C}(\tau)$.

Let now consider the case when the freestream temperature remains constant and heat generation takes place in a thin layer positioned at $x=0$, which models the case when a thin heater foil is attached to the surface. This case is described by the following boundary conditions:

$$\begin{aligned} &\xi=0: \quad \dot{\boldsymbol{Q}}_\mathrm{w}=\dot{\boldsymbol{Q}}_\mathrm{w,a}+\dot{\boldsymbol{\Phi}}_\mathrm{w}(\tau)=h[T(0,\tau)-T_\mathrm{g}]+q(0,\tau)\\ &\xi=1: \quad q(1,\tau)=0 \end{aligned} \tag{18}$$

where $\dot{\boldsymbol{Q}}_\mathrm{w}$is the power generated per surface unit into the thin layer (which is supposed to be at uniform temperature equal to $T(0,\tau)$), $\dot{\boldsymbol{Q}}_\mathrm{w,a}$is the time average: $\dot{\boldsymbol{Q}}_\mathrm{w,a}=\lim_{\Upsilon\to\infty}\frac{1}{\Upsilon}\int_0^\Upsilon\dot{\boldsymbol{Q}}_\mathrm{w}(\tau)\,\mathrm{d}\tau$; and $\dot{\boldsymbol{\Phi}}_\mathrm{w}(\tau)$ the fluctuating component. Introducing the Fourier transform of $\dot{\boldsymbol{\Phi}}_w(\tau)$:

$$\dot{\boldsymbol{\Phi}}_\mathrm{w}(\tau)=\int_{-\infty}^{+\infty}\mathrm{e}^{\mathrm{i}\omega\tau}\Psi(\omega,\xi)\,\mathrm{d}\omega$$

and applying the boundary conditions (18) one obtains for the steady components

$$\begin{aligned} &T_\mathrm{a}(\xi)=T_0\to q_\mathrm{a}(\xi)=0\\ &\dot{\boldsymbol{Q}}_\mathrm{g}=h[T_0-T_\mathrm{g}] \end{aligned} \tag{19}$$

and for the fluctuating components

$$\Psi(\omega)=\frac{k}{L}(1+\mathrm{i})\sqrt{\frac{\omega}{2}}[S_-(\omega)-S_+(\omega)]+h[S_-(\omega)+S_+(\omega)] \tag{20}$$

Using again Eq. (11) (obtained from the boundary conditions at $\xi=1$):

$$\Psi(\omega)=\frac{k}{L}S(\omega,0)\left\{Bi+(1+i)\sqrt{\frac{\omega}{2}}Q(\omega)\right\}$$

where again $Bi = hL/k$ and $Q(\omega)$ is defined by Eq. (14). It is now straightforward to obtain the relation similar to Eq. (17):

$$Bi = -\sqrt{\frac{\omega}{2}}\{K^-(\omega) + K^+(\omega)W_\Psi(\omega)\}$$

with now

$$W_\Psi(\omega) = \frac{\mathrm{Re}[S(\omega,0)\Psi^*(\omega)]}{\mathrm{Im}[S(\omega,0)\Psi^*(\omega)]}$$

where Ψ^* is the complex conjugate of Ψ. As for the previous case, defining the temperature–power cross-correlation

$$\mathscr{C}_\Psi(\tau) = \int_{-\infty}^{+\infty} \theta(0, t+\tau)\dot{\Phi}_\mathrm{w}(t)\,\mathrm{d}t$$

the convolution theorem for Fourier transform gives

$$\mathscr{C}_\Psi(\tau) = \int_{-\infty}^{+\infty} \mathrm{e}^{\mathrm{i}\omega\tau} S(\omega,0)\Psi^*(\omega)\,\mathrm{d}\omega$$

thus also $W_\Psi(\omega)$ can be evaluated from the real and imaginary components of the Fourier transform of $\mathscr{C}_\Psi(\tau)$.

As the two cases are so similar, in the following sections only the first one (varying freestream temperature) will be analysed and all the results are readily applicable to the second one.

3. Effect of time dependence of the convective coefficient

It was shown [14] that in transient methods the heat transfer coefficient may vary with time. To explicitly show this dependence in case of periodic regime, consider the boundary condition (3), where each parameter was split into steady and fluctuating parts (see Eqs. (4) and (5))

$$q_\mathrm{a}(0) + \varphi(0,\tau) = [h_\mathrm{a} + \eta(\tau)][T_\mathrm{g,a} + \theta_\mathrm{g}(\tau) - T_\mathrm{a}(0) - \theta(0,\tau)] \tag{21}$$

with $h(\tau) = h_\mathrm{a} + \eta(\tau)$ and $h_\mathrm{a} = \langle h(\tau)\rangle$, brackets $\langle\,\rangle$ indicate the time average: $\langle f\rangle = \lim_{\Upsilon\to\infty}\frac{1}{\Upsilon}\int_0^\Upsilon f(\tau)\,\mathrm{d}\tau$.

Taking the average of each side of Eq. (21)

$$q_\mathrm{a}(0) = h_\mathrm{a}[T_\mathrm{g,a} - T_\mathrm{a}(0)] + \langle\eta(\tau)[\theta_\mathrm{g}(\tau) - \theta(0,\tau)]\rangle \tag{22}$$

Consider now the case of fluctuating gas temperature and adiabatic condition at $x = L$ (but a similar discussion can be done for other boundary conditions), then $q_\mathrm{a}(0) = 0$, which implies

$$T_\mathrm{g,a} - T_\mathrm{a}(0) = -\frac{\langle\eta(\tau)[\theta_\mathrm{g}(\tau) - \theta(0,\tau)]\rangle}{h_\mathrm{a}} \tag{23}$$

i.e., due to the correlation between fluctuating temperature and heat transfer coefficient, the average wall and gas temperatures will differ by an amount depending on the characteristics of the fluctuating fields.

Inserting Eq. (22) in (21)

$$\varphi(0,\tau) = h_\mathrm{a}[\theta_\mathrm{g}(\tau) - \theta(0,\tau)] + \{\eta(\tau)[T_\mathrm{g,a} - T_\mathrm{a}(0)] + \eta(\tau)[\theta_\mathrm{g}(\tau) - \theta(0,\tau)] - \langle\eta(\tau)[\theta_\mathrm{g}(\tau) - \theta(0,\tau)]\rangle\} \tag{24}$$

the last term in brackets is the addition due to the time dependence of the heat transfer coefficient. For the case under consideration it can also be written as

$$\phi(\tau) = [h_\mathrm{a} + \eta(\tau)][T_\mathrm{g,a} - T_\mathrm{a}(0)] + \eta(\tau)[\theta_\mathrm{g}(\tau) - \theta(0,\tau)]$$

Now, to estimate the weight of $\phi(\tau)$ respect to $h_\mathrm{a}[\theta_\mathrm{g}(\tau) - \theta(0,\tau)]$ in Eq. (24), the amplitude of the coefficient fluctuation and the correlation between coefficient and temperature fluctuations should be known. To the author knowledge, there not exist available experimental or numerical results on such effect (as the results reported in [14] were obtained for transient non-periodic heating); it can only be speculated that the effect of time variation of the convective coefficient may be smaller for turbulent boundary layer than for the laminar one as this happens for the transient non-periodic case [14]. Due to this lack of knowledge, in the rest of this paper such possible effect will be neglected, and it should be noticed that practically all the commonly used methods to evaluate the heat transfer coefficient with transient methods rely on the assumption that heat transfer coefficient is not influenced by the temperature unsteadiness.

4. Uncertainties and sensitivity analysis

There may be various sources of uncertainty when extracting the value of Bi from measured spectra. First of all, Eq. (17) shows how an error on the evaluation of $W(\omega)$ will produce an error in evaluating Bi. Precisely, the relative error ($\varepsilon_{Bi}^{(W)}$) on Bi will be related to the relative error (ε_W) on W as

$$\varepsilon_{Bi}^{(W)} = \frac{W}{Bi}\frac{\mathrm{d}Bi}{\mathrm{d}W}\varepsilon_W = \left[1 + \sqrt{\frac{\omega}{2}}\frac{K^-(\omega)}{Bi}\right]\varepsilon_W$$

and Fig. 1 shows the ratio $\varepsilon_{Bi}^{(W)}/\varepsilon W$ as a function of ω and Bi. It is then evident that there exists a sort of "frequency threshold" for each value of Bi above which the errors in evaluating Bi grows rapidly and Fig. 2 reports the values of W for which $\varepsilon_{Bi}^{(W)}/\varepsilon W = 2$, for a wide range of Bi. This effect can also be appreciated through Fig. 3, showing the values of W as a function of ω for different values of Bi. The threshold is there defined by the line on which all curves collapse.

Another source of error can be related to the uncertainty on the measurement of wall thickness or wall

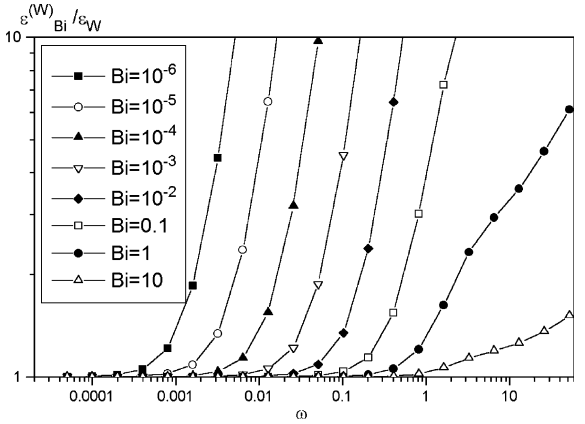

Fig. 1. Ratio of relative errors on Bi and W as a function of non-dimensional frequency ω and Bi.

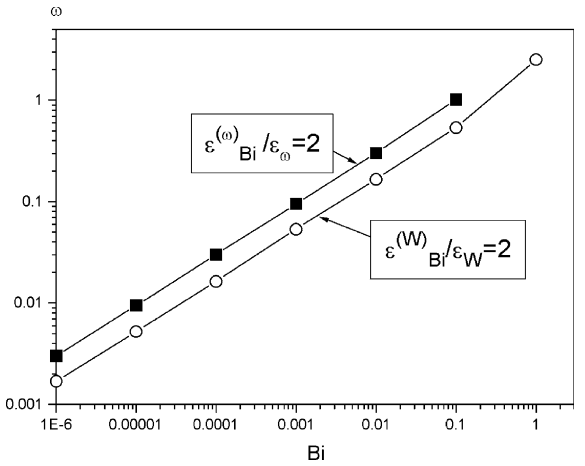

Fig. 2. Frequency threshold for errors due to uncertainty on evaluating W from Fourier transform ($\varepsilon_{Bi}^{(W)}/\varepsilon_W$) and uncertainty on evaluating ω from material properties ($\varepsilon_{Bi}^{(\omega)}/\varepsilon_\omega$).

thermal properties. Again the separate effects of those sources can be evaluated through the relation

$$\varepsilon_{Bi}^{(\omega)} = \frac{\omega}{Bi}\frac{\mathrm{d}Bi}{\mathrm{d}\omega}\varepsilon_\omega$$

where ε_ω is the relative error on ω due to uncertainties in evaluating α or L, then $\varepsilon_\omega = -\varepsilon_\alpha$ or $\varepsilon_\omega = 2\varepsilon_L$ where ε_α and ε_L are the relative uncertainties on α and L respectively. Fig. 4 shows the relation $Bi(\omega)$ for different values of W (Eq. (17)); it can be appreciated how there exists values of ω for which the derivative $\mathrm{d}Bi/\mathrm{d}\omega$, and then $\varepsilon_{Bi}^{(\omega)}$, is nil. Around that region the method is insensitive to uncorrect evaluation of ω (i.e. of α and L). Fig. 5 shows the values of $\varepsilon_{Bi}^{(\omega)}/\varepsilon_\omega$ and again the existence of a frequency threshold (depending on the value of Bi) above which errors may become too large. Fig. 2 reports

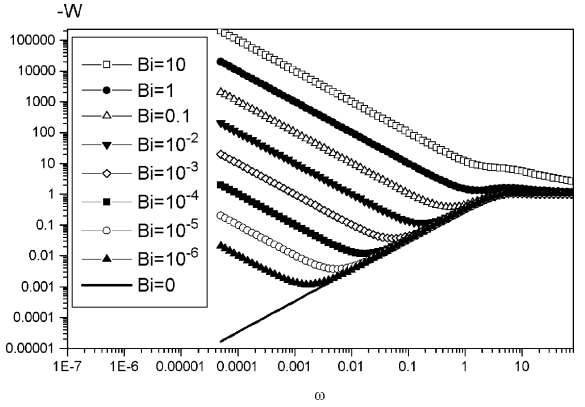

Fig. 3. The ratio $-W = -\frac{\mathrm{Re}\{S(\omega,0))G^*\}}{\mathrm{Im}\{S(\omega,0))G^*\}}$ vs. non-dimensional frequency ω.

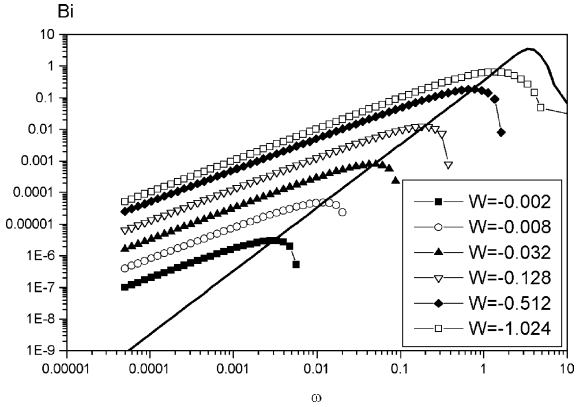

Fig. 4. Plot of Bi vs. ω for different values of W (Eq. (3.15)).

also the values of ω for which $\varepsilon_{Bi}^{(\omega)}/\varepsilon_\omega = 2$, for a wide range of Bi; it can be appreciated how this constraint is weaker than that imposed by the uncertainty on the values of W.

The measured temperatures may also be affected by random noise, produced by the devices used to acquire the signals, and this affects the signals Fourier transforms and then the evaluation of Bi. But there may be other causes like the fact that the slab is never perfectly adiabatic in $x = L$ and this may introduce a deterministic bias on Bi evaluation. These sources of error will be analysed here as they are certainly among the most significant ones that may bias the evaluation of Bi.

4.1. Random noise

To better analyse the effect of random noise superimposed to the actual measured temperature values, a numerical simulation was implemented. A finite

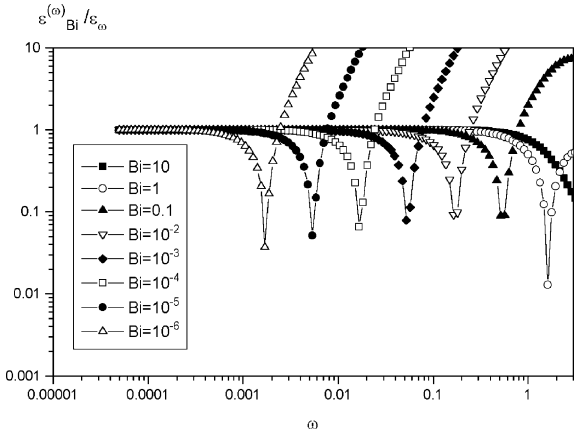

Fig. 5. Ratio of relative errors on Bi and ω as a function of non-dimensional frequency ω and Bi.

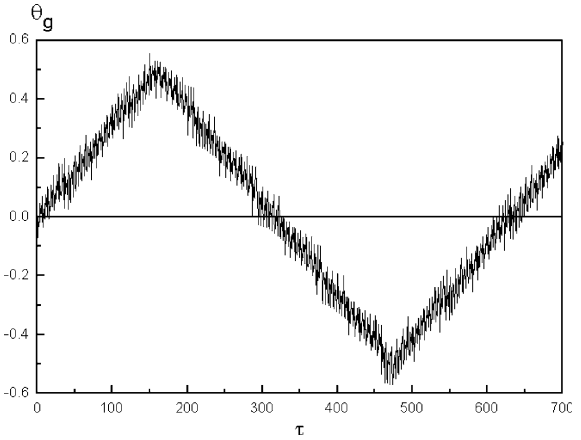

Fig. 7. Freestream temperature with superimposed a white noise ($\sigma_g = 0.02$).

differences discretisation and explicit method were used. Tests where performed to check the accuracy, non-dimensional frequency ω was varied in a wide range (10^{-3}–10) as well as the imposed value of Bi (10^{-4}–10). Accuracy depends on both parameters, numerical errors in evaluating Bi by the procedure above described increases when Bi decreases and ω increases (see Fig. 6 for an example). However, a proper choice of other parameters like the mesh size and the time step can always improve the accuracy to the desired value, obviously increasing the computational time. The analysis of the random noise effects was performed with parameters set in order to get a computational error in evaluating the Bi form spectra (Eq. (17)) always lower than 10^{-4}. White noises of different intensities were added to the freestream and wall temperature signals and the resulting time series were used to compute Fourier transforms and to evaluate Bi. The deterministic freestream temperature signal was a periodic linear ramp (see Fig. 7). The added disturbances were white noises (random noise with Gaussian distribution) and their intensities (the rms of the distributions: σ_g for the freestream and σ_w for the wall surface) were varied between 0 and 0.32 times the signal amplitude for both freestream and wall temperature signal. Due to information redundancy, Bi can be evaluated taking the average of values relative to many frequencies but accuracy decreases strongly when ω increases above the threshold previously mentioned (which depends on Bi), Fig. 8 shows a result of the numerical simulation (for $Bi = 0.1$): the value of the ratio $\frac{Bi_{meas}}{Bi_{th}}$ (where Bi_{meas} is the calculated value of Bi whereas Bi_{th} is the correct one) is plotted vs. the non-dimensional frequency ω and it remains close to 1 only for $\omega < 0.1$. Fig. 9 shows the results of the simulations in terms of the

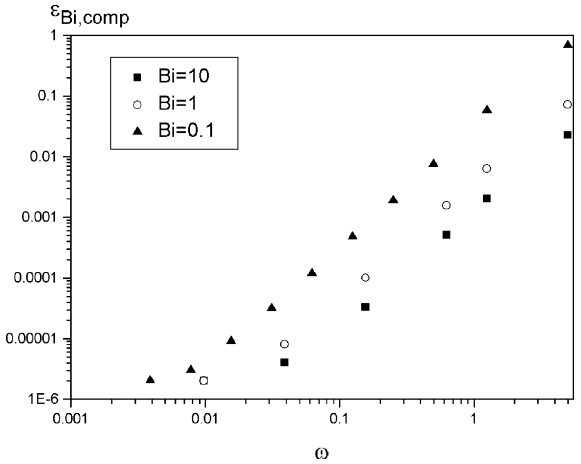

Fig. 6. Uncertainty on evaluating Bi from numerical simulation due to computational errors.

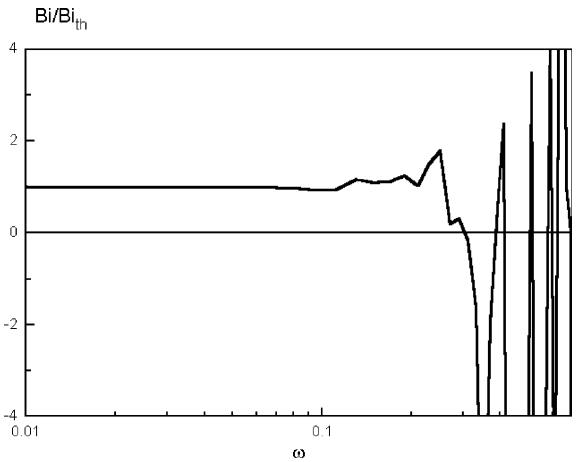

Fig. 8. Dependence of $\frac{Bi}{Bi_{th}}$ on non-dimensional frequency ω.

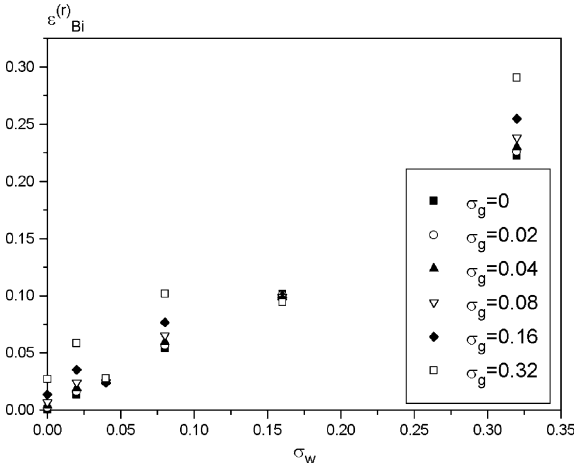

Fig. 9. Effect of random noise on accuracy in evaluating *Bi*.

effect of random noise on the relative error in valuating *Bi* (again for $Bi = 0.1$). $\varepsilon^{(r)}_{Bi}$ was calculated as: $\varepsilon^{(r)}_{Bi} = |\frac{\bar{Bi}}{Bi} - 1|$ where $\bar{Bi}$ is the average taken over all the values for $\omega < 0.1$. It is interesting to observe that the resulting relative error is comparatively confined and it can be strongly diminished by using lower ω, for example: by using only the values of *Bi* for $\omega < 0.05$ the relative error $\varepsilon^{(r)}_{Bi}$ was always lower than 0.02 for all the range of σ_g and σ_w above mentioned.

4.2. Non-adiabatic slab

In this case the boundary conditions become

$$\xi = 0: \quad q(0,\tau) = h[T_g(\tau) - T(0,\tau)]$$

$$\xi = 1: \quad q(1,\tau) = h_1(T(1,\tau) - T_{g1})$$

where T_{g1} is the (constant) temperature of the fluid in contact to the wall at $x = L$ and h_1 is the convective heat transfer coefficient. These constraints impose on the steady components the following conditions (to be compared to Eq. (10)):

$$q_a(\xi) = \text{const.} = \frac{\Delta T_g}{R_L}$$
$$T_a(\xi) = a + b\xi \tag{25}$$

where $\Delta T_g = T_g - T_{g1}$, $R_L = (\frac{1}{h} + \frac{L}{k} + \frac{1}{h_1})$, $a = T_{g1} + \Delta T_g \frac{(\frac{1}{h_1} + \frac{L}{k})}{R_L}$, $b = -\Delta T_g \frac{L}{kR_L}$. The boundary condition in $\xi = 1$ gives, for the Fourier transform of the fluctuating components

$$\frac{k}{L}(1+\mathrm{i})\sqrt{\frac{\omega}{2}}[S_-(\omega)E_-(\omega) - S_+(\omega,1)E_+(\omega,1)]$$
$$= h_1[S_-(\omega)E_-(\omega,1) + S_+(\omega)E_+(\omega,1)]$$

where Eq. (25) were used, and then

$$S_+(\omega) = S_-(\omega)\frac{E_-(\omega,1)}{E_+(\omega,1)}H(\omega,Bi_1) \tag{26}$$

with $Bi_1 = \frac{h_1 L}{k}$, and

$$H(\omega,Bi_1) = \frac{2\sqrt{\frac{\omega}{2}} - Bi_1(1-\mathrm{i})}{2\sqrt{\frac{\omega}{2}} + Bi_1(1-\mathrm{i})} \tag{27}$$

Eq. (26) should be compared to (11), noticing that $H(\omega,0) = 1$.

The boundary condition in $\xi = 0$ becomes now:

$$G(\omega) = S(\omega,0)\left\{\frac{(1+\mathrm{i})}{Bi}\sqrt{\frac{\omega}{2}}Q_1(\omega,Bi_1) + 1\right\}$$

where

$$Q_1(\omega,Bi_1) = \frac{E_+(\omega,1) - E_-(\omega,1)H(\omega,Bi_1)}{E_+(\omega,1) + E_-(\omega,1)H(\omega,Bi_1)} \tag{28}$$

and then

$$Bi = -\sqrt{\frac{\omega}{2}}\{K_1^-(\omega,Bi_1) + K_1^+(\omega,Bi_1)W(\omega,Bi_1)\} \tag{29}$$

with $K_1^{\pm}(\omega,Bi_1) = [\mathrm{Re}(Q_1(\omega,Bi_1)) \pm \mathrm{Im}(Q_1(\omega,Bi_1))]$. Again, Eq. (29) should be compared to Eq. (17), valid for the adiabatic case.

It is now possible to evaluate the relative error obtained evaluating *Bi* by using Eq. (17) instead of (29):

$$\varepsilon_{na} = \frac{Bi^{err}}{Bi} - 1 = \frac{\{K^-(\omega) + K^+(\omega)W(\omega,Bi_1)\}}{Bi} - 1 \tag{30}$$

with W evaluated from Eq. (29): $W(\omega,Bi_1) = -\left\{\frac{Bi}{\sqrt{\frac{\omega}{2}}K_1^+(\omega,Bi_1)} + \frac{K_1^-(\omega,Bi_1)}{K_1^+(\omega,Bi_1)}\right\}$.

Fig. 10 shows the dependence of this uncertainty to ω, *Bi* and Bi_1. The asymptotic value for $\omega \to 0$ can be evaluated (see Appendix A) obtaining

$$\lim_{\omega\to 0}\varepsilon_{na} = \beta\frac{[2\beta Bi^2 + 3Bi(1+\beta) + 3]}{(\beta^2 Bi^2 + 3\beta Bi + 3)} \tag{31}$$

with $\beta = \frac{Bi_1}{Bi}$ and Fig. 11 shows such dependence. It is clear that errors become small for larger values of ω (where, however, the other types of uncertainties become large, see Fig. 1 for example) as in such case the adiabatic slab condition is approached ($H(\omega,Bi_1) \to 1$). For small values of ω, the uncertainty due to the non-adiabatic condition is given by Eq. (31) and becomes large for *Bi* larger than about 0.5.

As a result of this analysis, it appears that, in order to minimize the sources of errors, the non-dimensional frequency ω should be maintained in the region indicated in Fig. 2 and that *Bi* should not be too small but kept smaller than 0.5 (through a proper choice of material properties and slab thickness).

5. The case of sinusoidal varying temperature

Consider the case when the gas temperature is periodically varied with: $T_g(t) = A\sin(\omega_0 t)$. The solution can

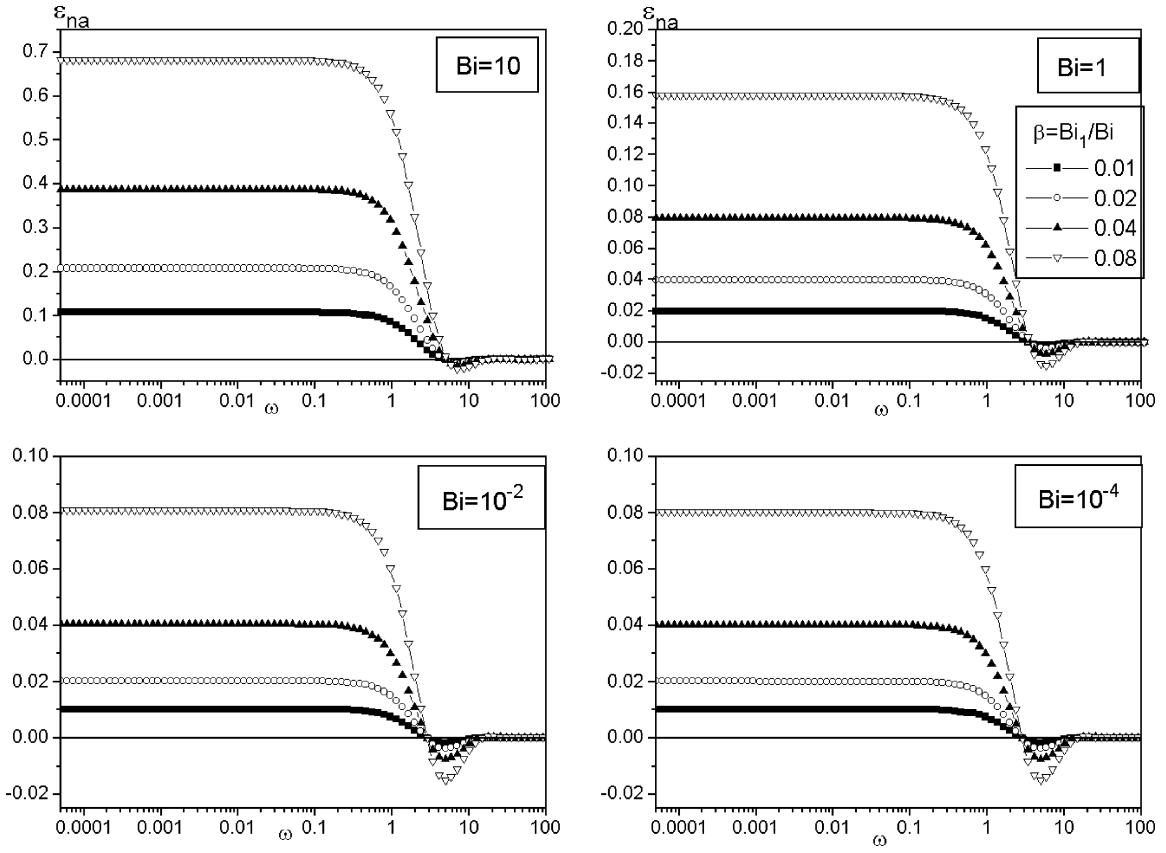

Fig. 10. Effect of non-adiabatic slab on accuracy in evaluating *Bi*.

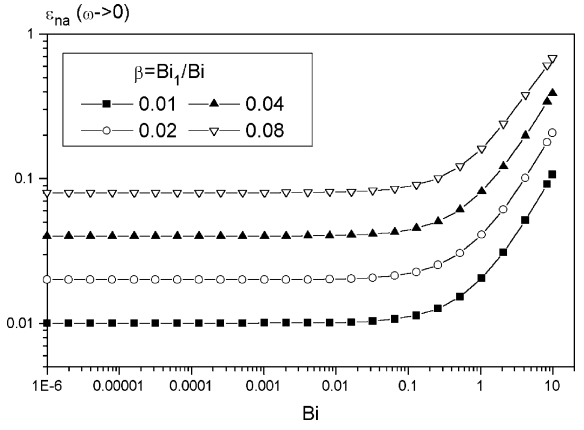

Fig. 11. Limit for $\omega \to 0$ of the error due to non-adiabatic slab condition.

be obtained as a particular case of the general problem above analysed by setting: $\mathrm{Re}\{G\} = 0$, $\mathrm{Im}\{G\} = -A\delta(\omega - \omega_0)$, where $\delta(\omega)$ is the Dirac–delta function, and taking the real part of the solution, then

$$S_\mathrm{r} = \mathrm{Re}\{S(\omega,0)\} = \frac{-K^+(\omega)}{\left\{\frac{Bi}{\sqrt{\frac{\omega}{2}}} + K^-(\omega)\right\}^2 + \{K^+(\omega)\}^2} A\delta(\omega-\omega_0) = Z_\mathrm{r}\delta(\omega-\omega_0)$$

$$S_\mathrm{i} = \mathrm{Im}\{S(\omega,0)\} = \frac{-\left\{\frac{Bi}{\sqrt{\frac{\omega}{2}}} + K^-(\omega)\right\}}{\left\{\frac{Bi}{\sqrt{\frac{\omega}{2}}} + K^-(\omega)\right\}^2 + \{K^+(\omega)\}^2} A\delta(\omega-\omega_0) = Z_\mathrm{i}\delta(\omega-\omega_0)$$

Now the solution for the surface temperature is

$$T(0,t) = \mathrm{Re}\left\{\int_{-\infty}^{+\infty} \mathrm{e}^{\mathrm{i}\omega t} S(\omega,0)\,\mathrm{d}\omega\right\} = Z_\mathrm{r}\cos(\omega t) - Z_\mathrm{i}\sin(\omega t) = \sin(\omega t + \phi)$$

where

$$\tan(\phi) = -\frac{Z_\mathrm{r}}{Z_\mathrm{i}} = -\frac{K^+(\omega_0)}{\left\{\frac{Bi}{\sqrt{\frac{\omega_0}{2}}} + K^-(\omega_0)\right\}}$$

from which the relation for sinusoidal varying gas temperature can be recovered

$$Bi = -\sqrt{\frac{\omega_0}{2}}K^-(\omega_0)\left\{1 + \frac{K^+(\omega_0)}{K^-(\omega_0)}\tan^{-1}(\phi)\right\}$$

which generalises, to the case of finite thickness slab, the well-known equation (valid for semi-infinite solid)

$$h = -k\sqrt{\frac{\omega_0'}{2\alpha}}\{1 + \tan^{-1}(\phi)\}$$

The above uncertainty analysis can be easily applied to this particular case too. It should be noticed that a similar result can be obtained for the case of constant freestream temperature and surface heat generation where $\dot{\Phi}_w(\tau) = B\sin(\omega_0\tau)$.

6. Conclusions

The proposed data reduction technique would allow to measure the convective heat transfer coefficient through the evaluation of the Fourier transform of simultaneously measured freestream and surface wall temperatures (or heating power and surface temperature). Any wave shape can be used to heat-up the stream (or the wall surface) and the method yields information redundancy on heat transfer coefficient, giving the possibility of checking the consistency of the results. The sensitivity analysis shows that, to reduce uncertainties, the non-dimensional frequency should be kept below a threshold value which depends on the range of the coefficient to be measured and this can be obtained by proper choices of the slab thickness and material and freestream heating period. The effect of noise on the measured temperature signals does not appears to be critical, as far as the signal to noise ratio is high. The effect of non-adiabatic back surface can become critical for large values of Bi but it can again be controlled by a proper choice of the slab material and thickness.

Appendix A

Substituting the value of W obtained from Eq. (29) into Eq. (30):

$$\varepsilon_1 = \frac{Bi^{\mathrm{err}}}{Bi} - 1 = \frac{-\sqrt{\frac{\omega}{2}}\{K^-(\omega) + K^+(\omega)W(\omega, Bi_1)\}}{Bi} - 1$$
$$= \frac{-\sqrt{\frac{\omega}{2}}K^-(\omega) + \frac{K^+(\omega)}{K_1^+(\omega,Bi_1)}\left\{Bi + \sqrt{\frac{\omega}{2}}K_1^-(\omega, Bi_1)\right\} - Bi}{Bi}$$

the limit for $\omega \to 0$ can be evaluated. In fact

$$\lim_{\omega\to 0}\sqrt{\frac{\omega}{2}}K^-(\omega) = 0$$

and

$$\lim_{\omega\to 0}\sqrt{\frac{\omega}{2}}K_1^-(\omega, Bi_1) = \frac{Bi_1}{1 + Bi_1}$$

and

$$\lim_{\omega\to 0}\frac{K^+(\omega)}{K_1^+(\omega, Bi_1)} = \frac{3(Bi_1 + 1)^2}{(Bi_1^2 + 3Bi_1 + 3)}$$

obtained applying repeatedly De L'Hospital rule. Then, introducing $\beta = \frac{Bi_1}{Bi}$:

$$\lim_{\omega\to 0}\varepsilon_1 = \beta\frac{[2\beta Bi^2 + 3Bi(1+\beta) + 3]}{(\beta^2 Bi^2 + 3\beta Bi + 3)}$$

that, for small values of Bi becomes equal to β.

References

[1] P.T. Ireland, T.V. Jones, The measurements of heat transfer coefficients in blade cooling geometries, in: AGARD Conference Proceedings No. 390, Paper 28, 1985.

[2] P.T. Ireland, T.V. Jones, Detailed measurements of heat transfer on and around a pedestal in fully developed passage flow, in: Proceedings of the 8th International Heat Transfer Conference Proceedings, vol. 3, 1986, pp. 975–980.

[3] R.J. Clifford, T.V. Jones, S.T. Dunne, Techniques for obtaining detailed heat transfer coefficient measurements within gas turbine blades and vane cooling passages, ASME Paper 83-GT-58, 1983.

[4] D.E. Metzger, E.E. Larson, Use of melting point surface coating for local convective heat transfer measurements in rectangular channel flows with 90-deg turns, ASME J. Heat Transfer 108 (1986) 48–54.

[5] D.E. Metzger, R.S. Bunker, G. Bosch, Transient liquid crystal measurement of local heat transfer on a rotating disc with jet impingement, ASME J. Turbomach. 113 (1991) 52–59.

[6] J.E. O'Brien, R.J. Simoneau, J.E. LaGraff, K.A. Morehaouse, Unsteady heat transfer and direct comparison for steady-state measurements in a Rotor-wake experiment, in: 8th International Heat Transfer Conference Proceedings, 1986, pp. 1243–1248.

[7] T.V. Jones, S.A. Hippensteele, High-resolution heat transfer coefficient map applicable to compound curve surfaces using liquid crystals in a transient wind tunnel, Development in Experimental Technique in Heat Transfer and Combustion, ASME Heat Transfer Division Conference Proceedings, vol. 71, 1987, pp. 1–9.

[8] J.W. Baughn, X. Yan, A preheated wall transient method for measurements of the heat transfer to an impinging jet, Eurotherm Seminar 25, 1991, pp. 1–7.

[9] J. Von Wolfersdorf, R. Hoecker, T. Sattelmayer, A hybrid transient step-heating heat transfer measurement technique using heater foils and liquid-crystal thermography, J. Heat Transfer 115 (1993) 319–323.

[10] J.W. Baughn, J.E. Mayhew, M.R. Anderson, R.J. Butler, A periodic transient method using liquid crystals for the measurements of local heat transfer coefficients, J. Heat Transfer 120 (3) (1998) 772–777.

[11] W.O. Turnbull, P.H. Oosthuizen, A new experimental technique for measuring surface heat transfer coefficient using uncalibrated liquid cristals, in: Proceedings ASME International Mechanical Engineering Congress, Heat Transfer Division, vol. 364 (4), 1999, pp. 121–126.
[12] V. Ditkine, A. Proudnikov, Tranformation integrales et calcul operationnel, MIR, Moscow, 1982, pp. 16–18.
[13] I.N. Sneddon, Fourier Transforms, Dover, New York, 1995, pp. 23–27.
[14] R.J. Butler, J.W. Baughn, The effect of the thermal boundary conditions on transient method heat transfer measurements on a flat plate with a laminar boundary layer, J. Heat Transfer 118 (1996) 831–837.